Combustion Theory and Modelling, 2019
Vol. 23, No. 4, 748–770, https://doi.org/10.1080/13647830.2019.1588380

Quasi-steady combustion of normal-alkane droplets supported by Cool-Flame chemistry near diffusive extinction

Forman A. Williams[a*] and Vedha Nayagam[b]

[a]*Department of Mechanical and Aerospace Engineering, University of California at San Diego, La Jolla, California, USA;* [b]*Department of Mechanical and Aerospace Engineering, Case Western Reserve University, Cleveland, Ohio, USA*

(*Received 24 October 2018; accepted 19 February 2019*)

Two steady-state chemical-kinetic approximations are introduced into the apparently most relevant five cool-flame steps of the latest San Diego mechanism for *n*-heptane, supplemented by a sixth step chosen to capture the influence of hot-flame chemistry on the cool flame in that mechanism, in order to obtain an effectively four-step chemical-kinetic description for addressing quasi-steady combustion of normal-alkane droplets in the lower-temperature part of the negative-temperature-coefficient (NTC) range, where cool-flame extinction is observed to occur. A development paralleling the classical activation-energy-asymptotic (AEA) analysis of the partial-burning regime, accompanied by an approximate description of a distributed reaction, is then pursued to make predictions of the combustion process, accounting for the large Lewis numbers of the fuel and intermediate species for the first time. The predictions are compared with results of droplet-combustion experiments performed in the International Space Station (ISS), showing reasonable agreement between theory and experiment and pointing to some needed future improvements in values of rate parameters. In addition, the theory predicts, for the first time, a limiting oxygen index (LOI) for droplet combustion of normal alkanes, giving, for example, for heptane burning in oxygen-nitrogen mixtures at normal room temperature, a corresponding oxygen mole fraction on the order of 0.10 in the ambient atmosphere, below which cool-flame-supported combustion cannot occur.

Keywords: Asymptotic analysis; partial burning regime; cool flames; droplet combustion; extinction

1. Introduction

Autoignition of normal alkanes involves different chemical-kinetic mechanisms at high and low temperatures, with a temperature range in between, the negative-temperature-coefficient (NTC) range, over which ignition occurs in two stages, and within which, contrary to normal behaviour, the total ignition delay time increases with increasing temperature [1–3]. In homogeneous mixtures, transient cool flames occur in this intermediate temperature range, leading to the chemical mechanism being called cool-flame chemistry. Although cool-flame chemistry had been found to be of significance in autoignition of alkane droplets in heated atmospheres [4], it was not thought to occur in quasi-steady diffusion flames. Experiments performed in the International Space Station (ISS), however, led to the discovery of two-stage alkane droplet combustion in

*Corresponding author. Email: faw@ucsd.edu

which a hot-flame stage, after extinguishing through a radiant-heat-loss mechanism, was followed by a quasi-steady stage of combustion sustained by cool-flame chemistry [5], buoyancy-limited earthbound measurements not having allowed sufficient residence times for this phenomenon to develop in earlier droplet-combustion experiments. Considering possible relevance to concepts for enhancing the performance of internal-combustion piston engines [6,7], this discovery motivated many subsequent computational [8–13] and experimental [14–18] studies of alkane droplet combustion supported by cool-flame chemistry.

Nearly twenty years ago, a seminal investigation showed how rate-ratio-asymptotic analyses can be applied to a short *n*-heptane mechanism to explain the NTC behaviour observed in autoignition experiments [19]. The chemistry employed in that study, updated from 56 to 62 steps, as well as a somewhat larger mechanism, involving 770 steps among 159 species (less than one fourth the size of mechanisms currently prevalent in the literature), was later applied in a computational investigation of quasi-steady droplet combustion supported by cool-flame chemistry [20], the previously cited computational investigations being fully time-dependent rather than quasi-steady. A relevant observation, presented in that work [20], was the reasoning, through static-stability considerations, that the NTC behaviour is the essential stabilising influence, quasi-steady droplet combustion becoming statically unstable outside the NTC range. It was found in that study that, as the droplet diameter decreased, the flame temperature decreased, eventually reaching the low-temperature limit of the NTC range. Diffusive extinction of droplet combustion supported by cool-flame chemistry therefore does not arise from the usual competition between the rate of chemical heat release and the rate of diffusive energy loss through heat conduction but rather is a chemical-kinetic/heat-transfer instability phenomenon, arising from the characteristics of the cool-flame chemistry in the diffusive environment of the burning droplet. Conventional understanding of diffusive extinction therefore does not apply to flame extinction in the cool-flame stage of droplet combustion.

The 62-step chemical-kinetic mechanism employed in the above study, with further up-dated values of rate parameters, incorporating some (but not all) of the revisions reported in more recent work [21], was simplified not long ago to the maximum extent possible by introducing steady-state approximations for reaction intermediaries, to obtain a two-equation description to which activation-energy asymptotics (AEA) was applied to calculate quasi-steady flame structures and extinction conditions [22]. That analysis, which produced qualitative agreement with experimentally observed droplet extinction diameters, was based on an expansion about the crossover temperature that separates the low-temperature chemistry from the high-temperature chemistry in the NTC region [19], the same type of chemistry having been employed earlier [15] for correlation of data. Numerical estimates, however, indicate that extinction likely occurs below the temperature range of validity of an expansion about crossover. In the present paper, building on a low-temperature mechanism developed for propane by Prince and Williams [23], a mechanism that offers a more thorough description of the low-temperature chemistry is applied to study the combustion and extinction occurring at temperatures below the vicinity of the crossover temperature. Through the introduction of two chemical-kinetic steady-state approximations, a six-step mechanism is reduced to one that essentially consists of four steps, providing chemical-kinetic expressions to which the Liñán AEA analysis of the partial-burning regime [24] is applied, along with an approximate treatment of a distributed reaction, in an effort to obtain improved agreement between predictions and measurements of droplet combustion made in ISS.

Previous related asymptotic analyses, as well as the earlier quasi-steady computational study [20], introduced the approximation that all Lewis numbers were unity. The accuracy of this approximation is especially questionable for cool flames because their important intermediates are large molecules (larger than the original fuel molecule), with correspondingly small diffusion coefficients, unlike oxygen (for which a Lewis number of unity is a good approximation when the diluent is nitrogen). For this reason, the present work extends the analysis to account for non-unity Lewis numbers of the fuel and intermediates, showing how to take that effect into account within the context of a canonical transformation to a single mixture-fraction variable. The previous asymptotic analysis [22], which underpredicted observed droplet diameters at extinction, underpredicts them further with a Lewis-number correction, but the present results, which provide a quantitative evaluation of the magnitude of these Lewis-number influences, exhibit improvements in agreements associated with inclusion of these effects.

2. The chemistry

Extensive developments in low-temperature alkane chemistry, initiated more than twenty years ago [25], can be simplified considerably, as has been described in greatest detail for propane [23]. Conversion of the fuel F to an alkyl radical R is brought about primarily through H-atom abstraction by hydroxyl, a dominant radical that is sufficiently reactive to exhibit an accurate chemical-kinetic steady state. Different alkyl isomers are not distinguished in this simplified description of the first elementary step, the same constant value for the specific reaction-rate constant being taken for all fuels addressed. Although the rate constant for this step increases approximately quadratically with the temperature T [21], over the T range of interest that variation is negligible, at least within the accuracy of the present analysis, thereby motivating the selection of a constant value, as listed in the table below. The second elementary step in the low-temperature chemistry, namely the addition of an oxygen molecule to R, also taken to have the same constant specific reaction-rate constant for all R (twice the value for the H abstraction from F by OH), is assumed to be followed by rapid isomerisation from RO_2 to QOOH, an intermediate abbreviated here (as before [23]) by I. The third step in the present chemistry description is the second O_2 addition, producing a species previously [23] denoted by J, which, however, maintains an accurate steady state, enabling it to be eliminated from the mechanism, resulting in the O_2 addition to I directly producing OH plus an alkylketohydroperoxide [21], denoted by K both here and earlier [23]. The steady state for species J, along with its energetics, leads to a negative activation energy for this second oxygen addition step, essential to NTC behaviour and involving an appreciably large negative effective activation temperature, -8360 K. The fourth and final principal step in this description of the chemistry is the unimolecular decomposition of K, liberating another OH radical, along with other products, collectively denoted here by P's. This well-known key branching step in the low-temperature mechanism has a significantly large activation energy, characterised below by an activation temperature of 19,840 K.

The introduction of steady-state approximations for OH and R into this four-step mechanism would result in a convenient two-step mechanism for describing the low-temperature chemistry. Consequent predictions, however, are very inaccurate because they overestimate the concentration of K appreciably. There are two reasons for this overestimate. One is that, besides producing K, the intermediate I also decomposes, reducing its concentration. For reasonable quantitative accuracy, then, it is necessary to take into account the

unimolecular decomposition of I to the conjugate alkene and the hydroperoxyl radical [23], collectively denoted by Q's as the fifth step in the table. The rate parameters for the four middle steps in the table are taken from the most recent source [26]. A second additional quantitative effect is the further reduction in the K concentration caused by the reduction in the concentration of I associated with the fact that, even below the crossover temperature, some of the radical R is consumed by the high-temperature path, effectively reducing its concentration below what it otherwise would be in the low-temperature mechanism. This effect is taken into account by the sixth step, the unimolecular C-C bond breakage resulting in an alkene and a lower alkane radical, collectively denoted by S's in the table, where the rate parameters listed for this step represent the sum of the rates of the four unimolecular decomposition steps of R appearing in the up-dated San Diego mechanism [21].

The above table summarises the starting chemistry that has now been described. In the specific reaction-rate constant for the k'th step, $k_k = A_k\ \mathrm{e}^{-T_{ak}/T}$, the A_k factors in the table have units cm^3/mol s for the first three (bimolecular) steps and simply s^{-1} for the last three (unimolecular) steps, with T_{ak} in K.

Energetic considerations require further attention in this mechanism. If the energetics were to be tied directly to each of the six steps, then specific structures would have to be specified for R, I, K, and the various collections of products that appear. An interior unsatisfied carbon bond might best be selected for R and maintained for I, which, for heptane, for example, is $C_7H_{14}OOH$, while K is $OC_7H_{13}OOH$ (the double carbonyl bond placed at the beginning, following convention), with similar selections made for the other alkanes. For heptane, the collection of P's should be taken to be [21] CO + CH_2O + C_2H_4 + n-C_3H_7, while, for octane, C_2H_4 here may be replaced by C_3H_6, which is a species that may also be added to the heptane products to apply to decane; similar simplifications would be introduced for higher normal alkanes. The specific selections for the species not involving O atoms, however, would have relatively little influence on predictions, and, moreover, there is little point in considering these details because additional steps, not appearing in the table, such as further oxidation of the alkyl products arising in this mechanism, likely have significant energetic effects in the cool flame and so would have to be included. In addition, energetic consequences of the oxidation of the portion of R that is consumed by the hot-flame route are to be expected. It therefore seems better to treat the energetics empirically.

With ω_k denoting the rate of step k in Table 1, the steady-state approximation for OH inplies that $\omega_1 = \omega_3 + \omega_4$. The radical R also maintains an accurate steady state during the low-temperature chemistry, resulting in $\omega_1 = \omega_2 + \omega_6$. If the sixth step is neglected, then this removes the rate parameters of the first two steps in the table from the chemical-kinetic description, providing what is formally a three-step description, in which the intermediate

Table 1. The six reaction steps and associated values of rate parameters that have been selected for n-heptane.

Number	Reaction	A	T_a
1	F + OH →R + H_2O	1.0×10^{12}	0
2	R + O_2 →I	2.0×10^{12}	0
3	I + O_2 →K + OH	3.5×10^{7}	−8360
4	K →P's + OH	4.0×10^{13}	19,840
5	I →Q's	2.0×10^{12}	12,090
6	R →S's	3.2×10^{13}	15,110

I carries on the necessary branching through K. If the fifth and sixth steps both could have been neglected, then there would have been a simpler two-step description, but the predictions of that approximation have been found to be inaccurate, the associated reduction in the concentration of I in both of the steps 5 and 6 being important quantitatively although not qualitatively.

At the higher NTC temperatures, K begins to approach a steady state, defined by $\omega_3 = \omega_4$, in which its concentration is related to the concentrations of I and O_2 according to $[K] = [I][O_2]0.88\times10^{-6}\exp(28,200/T)$, but this condition, reducing the K concentration substantially as the temperature increases, becomes highly inaccurate as the low-temperature end of the NTC range, of interest here, is approached. The temperature decrease results in a transition of the overall rate of heat release from the negative temperature dependence of ω_3 to the positive temperature dependence of ω_4, thereby defining the extinction condition determined by the onset of instability. At high temperatures in the NTC range, the reverse of the step 2 (that produces I) becomes important and begins to equilibrate, and additional steps involving OH, associated with the high-temperature hydrogen-oxygen branching, increasingly compete with this low-temperature path, these complications eventually removing the system from the NTC range at a high enough temperature, the rates of steps 1 and 2 then entering, along with rate parameters for high-temperature branching steps. While these complications must be addressed to consider the entire NTC range, for the majority of the cool-flame droplet-combustion histories in the ISS experiments, the preceding maximally simplified chemical-kinetic description, involving six irreversible steps, should suffice.

According to the table, the net rate of production of species K is simply $\omega_3 - \omega_4$, independent of the steady-state approximations that have been introduced. Rate expressions for the other species are, however, affected by the steady states. After ω_1 is eliminated through application of the steady state for OH, the steady-state expression for R contains four terms, $\omega_2 + \omega_6 = \omega_3 + \omega_4$. Throughout this low-temperature range in particular, however, the rate of step 4 is negligible compared with the rate of step 3 in the R balance, and the rate of step 6 similarly is much smaller than the rate of step 2. An accurate truncation of the steady-state expression for R therefore is obtained by equating the rate of step 2 to the rate of step 3, thereby relating the concentration of R directly to that of I. There results an expression for the production rate of I, which is $\omega_2 - \omega_3 - \omega_5$ according to the table, but which, in view of the R steady state, is equivalent to $\omega_4 - \omega_5 - \omega_6$, with the last term of which becoming proportional to the I concentration through the truncated R steady state. This completes the specification of the rates to be employed for I and K in the analysis.

For fuel, application of the OH steady state yields as its production rate $-\omega_3 - \omega_4$, while, for oxygen, formal application of the steady-state relations produces the rate $-2\omega_3 - (\omega_4 - \omega_6)$, with the last term ($\omega_6$) accounting for the net rate reduction of oxygen consumption attributable to the continued presence of the high-temperature path. There is a net consumption of both of these reactants in the cool flame, and, unlike the intermediates R, I, and K, these reactants are present in high concentrations, so that the cool-flame chemistry does not modify their distributions very much from those of diffusion-controlled predictions in frozen flow. The dominant cool-flame effect on the concentrations of these reactants is a kink in the locally essentially linear profiles at the hottest point in the flame, a dip arising through fuel and oxygen consumption by step 4. The chemical source term for each of these reactants therefore may be approximated as $-\omega_4$, which indicates that they are consumed there in roughly equal molar amounts. In addition, since the heat release is dominantly associated with the K-consumption process of step 4 in the lower-temperature

part of the NTC range (the other steps shown being more nearly energetically neutral), in energy conservation the rate at which this energy is released is taken to be proportional to the rate of step 4, with an empirical constant of proportionality, this empiricism being dictated by the aforementioned uncertainty in the energetics.

3. Transport aspects of the formulation

The formulation of the droplet-combustion problem is based on the conservation equations for steady flow in spherical geometry. Since cool-flame temperatures are low enough that radiant-energy effects can be neglected, energy conservation is a balance of heat conduction, convection, and chemical heat release, and the chemistry is balanced by convection of chemical species and their molecular transport through diffusion. One complication concerning transport phenomena is that the species F, I, and K have low diffusion coefficients, so that consideration should be given to Lewis numbers greater than unity. Although this influence has not been included in earlier analytical studies, its likely importance has been indicated previously [20,22]. A fortunate simplification is that, excluding the products, diffusion of which does not enter into the analysis, essentially only two types of species are present in the system, from the viewpoint of transport properties. One type is the oxidiser O_2 and the inert N_2, for which Lewis numbers are essentially unity, and the other type is the larger molecules, all of which have Lewis numbers appreciably greater than unity, in fact definitely greater than $L=2$. This enables simplified analyses with good accuracy to be developed, a benefit not available when N_2 is replaced by He or Xe, causing the Lewis number of O_2 to differ significantly from unity, as in some previous ISS experiments[15,27].

Values of diffusion coefficients are available in the literature for normal alkanes but not for the intermediate species I and K. These high-Lewis-number species are present in small enough concentrations that their contributions to the thermal diffusivity through equipartition of energy can be neglected, enabling their Lewis numbers to be estimated from their diffusion coefficients. From literature data, that estimate produces approximately $L=3$ for heptane, with somewhat higher values for higher alkanes. It will be found later, however, that the value of the Lewis number of the fuel does not affect the most important results to be developed here, while the Lewis numbers of I and K are critical, diffusion of these intermediates playing central roles. The kinetic theory of gases indicates that diffusion coefficients vary approximately inversely with the square root of the molecular weight of the molecule, which results in estimated Lewis numbers of the intermediates formed through O_2 addition being closer to $L=4$. This higher value will be employed in later comparisons.

A further transport complication of possible importance is the Soret effect, which tends to drive the larger, heavier molecules away from the hotter regions [20,22]. A helpful aspect of the present problem is that the high-Lewis-number species have low enough concentrations in the reaction zone (mole fractions of 0.1 or less [20]) that they can be treated in the dilute limit in which their molecular-diffusion fluxes, including Soret, in the spherical co-ordinate system with radius r become proportional to $\mathrm{d}Y_i/dr + \alpha_i(Y_i/T)\mathrm{d}T/dr$, where the Y_i denote the mass fractions of each species i and α_i their thermal diffusion factors, which depend little on their concentrations or on temperature. Use has been made of this fact to account for Soret diffusion of H_2 [28], for which α_i is negative (while it will be positive for F, I, and K in the present problem). Given this form of the operator that includes

both Fick and Soret diffusion, introduction of the modified dependent variable $Y_i T^{\alpha_i}$ serves to include the Soret effect in a purely Fikian form [28]. When that is done in the present problem, especially for the important intermediate species I and for K in the analysis, it turns out that, because of the factor Y_i multiplying α_i, the Soret term becomes very small in comparison with the Fick term. For that reason, the complexity of the formulation is reduced from the outset by not including the Soret term.

4. The initial mathematical formulation

In the formulation the average molecular weight is approximated as being constant, equal to that of the ambient atmosphere, W_∞, so that the gas density ρ varies inversely with the temperature T, according to the adopted ideal gas law, and, in terms of the mass fraction Y_i of any species i and its molecular weight W_i, its concentration that appears in the reaction-rate expressions is $Y_i\rho/W_i$. With a Lewis number of unity for O_2 and N_2, the thermal diffusivity D is taken to be the binary diffusion coefficient of O_2 into N_2. Letting $4\pi\mu$ denote the quasi-steady mass-loss rate of the burning droplet, with the mass fractions of F, O_2, I, and K denoted by Y_F, Y_O, Y_I, and Y_K, respectively, through a development similar to that given in previous work [20], in view of the preceding discussion of the chemistry, the gas-phase conservation equations for these species can be shown to become

$$\mu\frac{\mathrm{d}Y_F}{\mathrm{d}r} = \frac{1}{L}\frac{\mathrm{d}}{\mathrm{d}r}\left(r^2\rho D\frac{\mathrm{d}Y_F}{\mathrm{d}r}\right) - r^2 W_F\omega_4, \tag{1}$$

$$\mu\frac{\mathrm{d}Y_O}{\mathrm{d}r} = \frac{\mathrm{d}}{\mathrm{d}r}\left(r^2\rho D\frac{\mathrm{d}Y_O}{\mathrm{d}r}\right) - r^2 W_O\omega_4, \tag{2}$$

$$\mu\frac{\mathrm{d}Y_I}{\mathrm{d}r} = \frac{1}{L}\frac{\mathrm{d}}{\mathrm{d}r}\left(r^2\rho D\frac{\mathrm{d}Y_I}{\mathrm{d}r}\right) + r^2 W_I(\omega_4 - \omega_5 - \omega_6), \tag{3}$$

and

$$\mu\frac{\mathrm{d}Y_K}{\mathrm{d}r} = \frac{1}{L}\frac{\mathrm{d}}{\mathrm{d}r}\left(r^2\rho D\frac{\mathrm{d}Y_K}{\mathrm{d}r}\right) + r^2 W_K(\omega_3 - \omega_4) \tag{4}$$

(where the Lewis number L can be allowed to have different values for different species). Conservation equations are not considered for inerts or product species because they clearly will not influence the other solutions. Similarly, with the specific heat at constant pressure c_p assumed constant and the previously discussed empirical heat release associated with step 4 written in terms of a temperature increment T_Q as $c_p W_\infty T_Q$ for notational convenience, the differential equation for energy conservation becomes

$$\mu\frac{\mathrm{d}T}{\mathrm{d}r} = \frac{\mathrm{d}}{\mathrm{d}r}\left(r^2\rho D\frac{\mathrm{d}T}{\mathrm{d}r}\right) + r^2 W_\infty T_Q\omega_4, \tag{5}$$

with T_Q to be obtained from considerations of oxygen consumption, there being additional fuel consumption in the chemistry that does not release heat.These are the five differential equations to be studied here. In calculating c_p, since fuel is the only species transported between the droplet surface and the flame (the region in which energy conservation is most important), the value to be selected is that of the fuel vapour at an intermediate temperature, following previous recommendations [29], that choice having been found to exert a notable influence on later predictions.

These equations are to be solved, subject to the given boundary conditions in the ambient atmosphere, identified by the subscript ∞ and applied at $r = \infty$, along with boundary conditions at the surface of the droplet, identified by the subscript s and applied at the droplet radius, $r = r_s$. The droplet is taken to be at a uniform temperature and to maintain evaporative equilibrium, with a sufficiently large heat of vaporisation and gas-phase fuel mole fraction that its temperature T_s can be approximated well as the normal boiling point of the fuel. Interphase species and energy conservation equations can then be written as

$$\begin{aligned}
\left(r_s^2 \rho \frac{D}{L} \frac{\mathrm{d}Y_F}{\mathrm{d}r}\right)_{r=r_s} &= -\mu(1 - Y_{Fs}),\\
\left(r_s^2 \rho D \frac{\mathrm{d}Y_O}{\mathrm{d}r}\right)_{r=r_s} &= \mu Y_{Os},\\
\left(r_s^2 \rho \frac{D}{L} \frac{\mathrm{d}Y_{I,K}}{\mathrm{d}r}\right)_{r=r_s} &= \mu Y_{Is,Ks},\\
\left(r_s^2 \rho D \frac{\mathrm{d}T}{\mathrm{d}r}\right)_{r=r_s} &= \mu T_L,
\end{aligned} \tag{6}$$

where the heat of vaporisation per unit mass for the fuel has been denoted by $c_p T_L$.

5. Transformation to convection-free form

Analysis can be facilitated by writing the conservation equations in convection-free form [24]. This normally involves the introduction of a conserved scalar such as a mixture fraction under the restriction that all Lewis numbers are unity, followed by transforming from r to this conserved scalar as the independent variable. Even though the Lewis number of the fuel (as well as of the important intermediates) is not unity in the present problem, so that convection must remain important for this species and the others with non-unity Lewis numbers, it has still been found to be useful to transform the problem to one with a hypothetical mixture fraction Z, having a Lewis number of unity, as the independent variable. This extension of the mixture-fraction formulation to account for some species having Lewis numbers different from unity, with an ancillary mixture fraction to be defined later, is novel and has not been introduced in previous investigations.The major mixture-fraction variable is defined by

$$\mu \frac{\mathrm{d}Z}{\mathrm{d}r} = \frac{\mathrm{d}}{\mathrm{d}r}\left(r^2 \rho D \frac{\mathrm{d}Z}{\mathrm{d}r}\right); \quad Z(\infty) = 0, \left(r^2 \rho D \frac{\mathrm{d}Z}{\mathrm{d}r}\right)_{r=r_s} = -\mu(1 - Z_s). \tag{7}$$

It is then readily shown [20] that

$$Z = 1 - \exp\left(-\int_r^\infty \frac{\mu}{r^2 \rho D} \mathrm{d}r\right), \tag{8}$$

so that

$$r = \left[\int_0^Z \frac{\rho D}{\mu\,(1 - Z)} \mathrm{d}Z\right]^{-1}, \tag{9}$$

and in terms of an r-dependent inverse time

$$\chi = 2D\left(\frac{\mathrm{d}Z}{\mathrm{d}r}\right)^2, \tag{10}$$

the convection and diffusion operators in (2) and (5) combine according to

$$\frac{\mu}{r^2}\frac{\mathrm{d}}{\mathrm{d}r} - \frac{1}{r^2}\frac{\mathrm{d}}{\mathrm{d}r}\left(r^2\rho D\frac{\mathrm{d}}{\mathrm{d}r}\right) = -\frac{\rho\chi}{2}\frac{\mathrm{d}^2}{\mathrm{d}Z^2}, \tag{11}$$

leading to linearity of solutions in Z space away from reaction regions for Lewis numbers of unity. Use of the condition at the droplet surface in (7) then conveniently extends the linearity in Z space to the full domain $0 < Z < 1$ [20]. The function $\chi(Z)$, the product of the thermal diffusivity and the squared magnitude of the gradient of Z, which approaches zero at $Z = 0$ and at $Z = 1$ according to its definition, achieving a maximum value somewhere between these two limits, is often called the scalar dissipation rate because in turbulent flow its average conditioned on the value of the scalar Z represents the rate of dissipation of fluctuations of Z at that value, but in the present context it would more properly represent the appropriate inverse time scale for heat conduction at the value of Z.

After the transformation to Z as the independent variable is made, the conservation equations become

$$\frac{\rho\chi}{2}\frac{\mathrm{d}^2T}{\mathrm{d}Z^2} = -w_T, \tag{12}$$

$$\frac{\rho\chi}{2}\frac{\mathrm{d}^2Y_O}{\mathrm{d}Z^2} = -w_O, \tag{13}$$

and

$$\frac{\rho\chi}{2L}\frac{\mathrm{d}^2Y_i}{\mathrm{d}Z^2} + \frac{L-1}{2L}\frac{\rho\chi}{1-Z}\frac{\mathrm{d}Y_i}{\mathrm{d}Z} = -w_i, \tag{14}$$

for i = F, I, K, in which the chemical source terms are

$$\begin{aligned} &w_T = W_\infty T_Q\omega_4, \quad w_O = -W_O\omega_4, \quad w_F = -W_F\omega_4, \\ &w_I = W_I(\omega_4 - \omega_5 - \omega_6), \quad w_K = W_K(\omega_3 - \omega_4). \end{aligned} \tag{15}$$

The boundary values in the ambient atmosphere, identified by the subscript ∞, are to be applied at $Z = 0$, and the boundary conditions at the droplet surface, given by (6), become

$$\begin{aligned} &(1-Z_s)\left(\frac{\mathrm{d}T}{\mathrm{d}Z}\right)_{Z=Z_s} = -T_L, \quad (1-Z_s)\left(\frac{\mathrm{d}Y_O}{\mathrm{d}Z}\right)_{Z=Z_s} = -Y_{Os}, \\ &(1-Z_s)\left(\frac{\mathrm{d}Y_F}{\mathrm{d}Z}\right)_{Z=Z_s} = L(1-Y_{Fs}), \quad (1-Z_s)\left(\frac{\mathrm{d}Y_i}{\mathrm{d}Z}\right)_{Z=Z_s} = -LY_{is} \end{aligned} \tag{16}$$

for $i = I,K$. Equations (12) through (16) provide a convenient formulation of the problem in mixture-fraction space.

6. Outer solutions

A thin reaction zone for the high-activation-energy steps 4, 5, and 6 is considered to be located in the vicinity of $Z = Z_f$, so that the variable Z can be stretched about $Z = Z_f$, where the temperature is highest, with the chemical reaction rates of those steps vanishing outside the range of this stretching. Since it is only step 4 that influences the temperature appreciably, the solution for $T(Z)$ outside this range, its outer solution, is linear in Z and, at the leading order in the analysis, it reaches the value $T = T_f$ at $Z = Z_f$, being continuous there in the first approximation. The solutions at leading order in the outer zones for all of the variables, also being continuous at this flame location, will be identified by the subscript f when evaluated at $Z = Z_f$.

With this notation, in view of the boundary conditions, the solutions to (12) in the outer zones are

$$\begin{aligned} T &= T_\infty + (T_f - T_\infty)(Z/Z_f), \quad \text{for } 0 < Z < Z_f, \\ T &= T_0 + (T_f - T_0)(1 - Z)/(1 - Z_f), \quad \text{for } Z_f < Z < 1, \end{aligned} \tag{17}$$

where use has been made of (16) to transfer the boundary conditions applicable at the droplet surface to conditions at $Z = 1$, the notation $T_0 = T_s - T_L$ having been introduced for the fictitious temperature at the centre of the droplet (which may be a negative absolute temperature but in fact is small but positive), so that the subscripts 0 and ∞ identify conditions at $r = 0$ and at $r = \infty$, respectively. It is worth emphasizing here that the values of T_f and Z_f are not fixed in advance, but the values of the other temperature constants that appear in (17) are known.

A similar solution applies to (13) for Y_O, namely,

$$\begin{aligned} Y_O &= Y_{O\infty} - (Y_{O\infty} - Y_{Of})(Z/Z_f), \quad \text{for } 0 < Z < Z_f, \\ Y_O &= Y_{Of}(1 - Z)/(1 - Z_f), \quad \text{for } Z_f < Z < 1, \end{aligned} \tag{18}$$

and this type of solution would also apply to (14) for Y_F if its Lewis number were unity. Unlike Y_O, however, instead of being constructed from a linear function of $(1 - Z)$, the solution for Y_F is obtained from a linear function of $(1 - Z)^L$, resulting in

$$\begin{aligned} Y_F &= Y_{Ff}[1 - (1 - Z)^L]/[1 - (1 - Z_f)^L], \quad \text{for } 0 < Z < Z_f, \\ Y_F &= 1 - (1 - Y_{Ff})[(1 - Z)/(1 - Z_f)]^L, \quad \text{for } Z_f < Z < 1. \end{aligned} \tag{19}$$

Similarly, from (14) and (16) for species I,

$$\begin{aligned} Y_I &= Y_{If}[1 - (1 - Z)^L]/[1 - (1 - Z_f)^L], \quad \text{for } Z < Z_f, \\ Y_I &= Y_{If}[(1 - Z)/(1 - Z_f)]^L, \quad \text{for } Z > Z_f. \end{aligned} \tag{20}$$

These solutions, accounting for Lewis numbers different from unity and not having previously been identified in the literature, work because none of the chemical source terms for these species in Equation (15) involve ω_3.

Unfortunately, because of the complexity of the expression for ω_3, accurate analytical solutions cannot be obtained for the concentration of species K in the outer zones, where this reaction has to be taken into account. A convenient way to address this difficulty, which has not been noticed previously, is to define an alternative mixture fraction $\tilde{Z}$ by (7)

with D replaced by D_i, the diffusion coefficient for the species to be considered. Then (8)–(10) follow for $\tilde{Z}$, with χ becoming $\tilde{\chi}$ in (10). It is necessary to relate $\tilde{Z}$ to the independent variable Z in the solution, and from (8) and the corresponding equation for $\tilde{Z}$, that relationship is found to involve an integral, unless the product ρD is constant. Since ρ varies inversely with T according to the ideal gas law, while D generally increases with T as a fractional power not very much less than unity, that approximation is reasonable and will be adopted henceforth. It then may be shown from (8) that $(1-\tilde{Z}) = (1-Z)^L$ and that $\tilde{\chi} = \chi L(1-Z)^{2(L-1)}$, providing the necessary relationships between the new mixture fraction and inverse residence time and the original ones.

Just as χ is a characteristic inverse time for heat conduction at a given value of Z, so is $\tilde{\chi}$ the characteristic inverse time for diffusion of the key reactants of steps 3 through 6 at a given value of $\tilde{Z}$. Therefore, in the outer zone, it is appropriate to approximate the rate ω_3 as $\omega_3 = C\rho\tilde{\chi}/W_K$, where C will be taken to be a constant in order to obtain an analytical solution. If, in the expression for ω_3, the prefactor 3.5×10^7 cm^3/mol s is denoted by B, and 8360 K is denoted by T_b, then the value of that constant should be selected to be a representative value of the function

$$C(Z) = [(W_K\rho)/(W_O W_I\tilde{\chi})]Y_O Y_I B\mathrm{e}^{T_b/T}. \tag{21}$$

Asymptotic analysis in the presence of a step having a negative activation energy has not been attempted before, and the present approximation, for the first time providing an analytical solution with a reaction occurring in the outer zones, is an approach having an accuracy that is yet to be determined but that must vary with the magnitude of the negative activation energy.

Different selections of the value of the constant C would likely be required to obtain reasonable values for different quantities, as would be expected from the observation that $C(Z)$ varies by more than an order of magnitude throughout the outer zones. For the present purposes the objective is to make a selection that best approximates the dependence of χ_f on T_f, because that dependence exerts the main influence on measurable quantities, so $\tilde{\chi}$ will be eliminated in favour of χ. Concentrations of reaction intermediaries, reflected in Y_{If} and in Y_{Kf}, for example, would require different choices for C and, moreover, should retain $\tilde{\chi}$ as a more pertinent inverse time scale, but those quantities are not measured. Considerations of the extent to which C should depend upon L for fitting $\chi_f(T_f)$ will be seen to affect the specification of the constant value for C.

The most convenient position for selecting a temperature at which to evaluate C is the flame, whence ρ_f and T_f will be used in (21) for those two variables appearing there. Suitable average values throughout the outer zones should be selected for Y_O and for Y_I. The oxygen concentration varies relatively smoothly in (21), decreasing on one side of the flame and increasing on the other, so the constant value Y_{Of} is an appropriate choice for its average. On the other hand, Y_I peaks at the flame and decreases to zero at both boundaries, so that $Y_{If}/2$ is a better choice for its average. The function $T(Z)$ also peaks at the flame, and the value of T_b is sufficiently large that the variation of T is expected to exert the dominant influence on the variation of $C(Z)$. Moreover, the temperature variation, being controlled by the thermal diffusivity, independent of L, should generate a Z dependence of T, driving the droplet response, that is governed by χ and does not depend strongly on L. The appearance here of $\tilde{\chi}$ instead of χ, however, produces a rather strong L dependence in $C(Z)$ for a given χ function, which therefore needs to be cancelled at the flame to produce a more nearly correct variation there. Given the preceding relationship between χ and $\tilde{\chi}$,

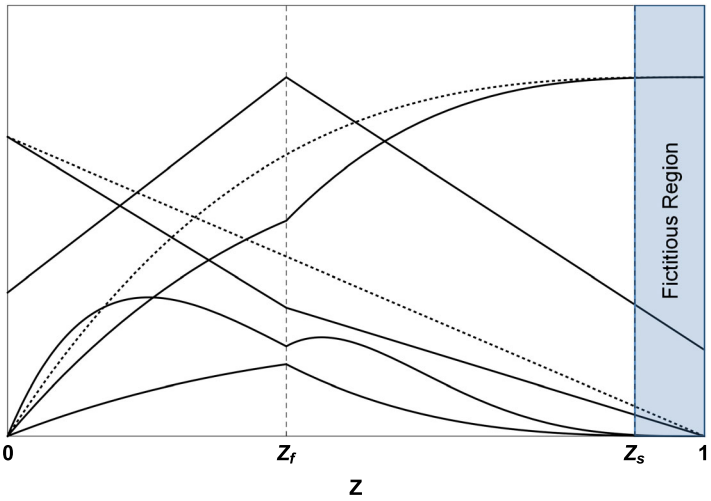

Figure 1. Schematic diagram of the flame structure.

this cancellation can be achieved by the selection

$$C = L(1 - Z_f)^{2L}[(W_K \rho_f)/(W_O W_I \tilde{\chi}_f)]Y_{Of}(Y_{If}/2)B\mathrm{e}^{T_b/T_f}, \tag{22}$$

which is to be used in the subsequent analysis.

With this selection, (14) for species K in the outer zone in this new mixture-fraction variable becomes simply $\mathrm{d}^2 Y_K/\mathrm{d}\tilde{Z}^2 = -2C$, the solution to which is

$$\begin{aligned} Y_K &= Y_{Kf}(\tilde{Z}/\tilde{Z}_f) + C\tilde{Z}(\tilde{Z}_f - \tilde{Z}), \quad \text{for } \tilde{Z} < \tilde{Z}_f, \\ Y_K &= Y_{Kf}[(1 - \tilde{Z})/(1 - \tilde{Z}_f)] - C[(1 - \tilde{Z})^2 + (1 - \tilde{Z}_s)^2] \\ &\quad + C[(1 - \tilde{Z}_f)^2 + (1 - \tilde{Z}_s)^2](1 - \tilde{Z})/(1 - \tilde{Z}_f), \quad \text{for } \tilde{Z} > \tilde{Z}_f. \end{aligned} \tag{23}$$

It may be noted that satisfaction of the boundary conditions requires that the value of $\tilde{Z}_s$ remains in the C term of this solution for the range $\tilde{Z} > \tilde{Z}_f$.

Figure 1 is a schematic diagram of the flame structure in the original mixture-fraction space according to this solution. The dashed curves shown there for the fuel and oxygen are the profiles that would occur under purely diffusive conditions without the reactant chemical consumption. The values of the mass fractions at the flame that appear in (18)–(20) and (23) are yet to be determined.

7. The inner problem

Unlike typical hot-flame problems, where T_f is determined by a condition of chemical equilibrium, becoming the adiabatic flame temperature if all Lewis numbers are unity, in partial-burning regimes there is a range of values of T_f, dependent on the chemical kinetics through the associated heat-release rate and residence time in the reaction zone. With the present chemistry, solutions will exist for a range of values of T_f, and the objective here is to find an analytical approximation to the solution that is valid in the vicinity of the minimum of the heat-release rate that occurs at the low-temperature end of the NTC region.

Therefore, solutions are investigated for values of T_f near the flame temperature at which this minimum occurs. This entails an AEA expansion of the inner zone in which steps 4, 5, and 6 occur while step 3 is too slow by comparison because the temperature there is too high for it to be of comparable importance.

The AEA expansion is based on the most important of the three steps that occur in this zone, the one (with the highest activation energy) that is responsible for the heat release. The prefactor 4.0×10^{13} s^{-1} for step 4 will be denoted by A, and given an activation temperature $T_a = 19{,}840$ K associated with AEA, the small expansion parameter is taken to be

$$\epsilon = T_f^2/[T_a(T_f - T_\infty)]. \tag{24}$$

The stretched mixture-fraction co-ordinate ζ, which serves as the independent variable in the inner zone, and the inner-zone temperature-decrement variable φ are then defined by

$$\zeta = (Z/Z_f - 1)/\epsilon, \varphi = (T_f - T)/[\epsilon(T_f - T_\infty)]. \tag{25}$$

Constants in these stretching formulas have been selected so that matching to the outer solution in (17) for $Z < Z_f$ will require that $\mathrm{d}\varphi/\mathrm{d}\zeta$ approached -1 as ζ approaches $-\infty$. In view of the stretching, at leading order the mass fractions may be expected to assume constant values Y_{if} throughout the inner zone.

In view of (12) and (15), the heat release in the inner zone is controlled by step 4, the rate of which is proportional to the constant K concentration, $Y_{Kf}\rho_f/W_K$ there, the reaction rate varying with temperature only in that zone. The inner equation then becomes

$$\mathrm{d}^2\varphi/\mathrm{d}\zeta^2 = \Delta \mathrm{e}^{-\varphi}, \tag{26}$$

where

$$\Delta = 2(W_\infty/W_K)(T_Q/T_a)[T_f/(T_f - T_\infty)]^2 Z_f^2 Y_{Kf} A \mathrm{e}^{-T_a/T_f}/\chi_f, \tag{27}$$

use having been made of (12), (15), (24), and (25). The value χ_f of the inverse time scale evaluated at the thin inner flame zone, which appears in this definition of the eigenvalue, specifies the relevant residence time of the fluid in this reaction zone for the present problem and will be termed the inverse residence time.

Given the form of (26), matching can be achieved only if the magnitudes of $\mathrm{d}T/\mathrm{d}Z$ are the same in the outer solutions on both sides of this inner zone. From (17) this can be shown to require that

$$Z_f = (T_f - T_\infty)/(2T_f - T_0 - T_\infty), \tag{28}$$

which serves to relate Z_f to T_f, a relationship that is needed in determining the dependence of T_f on χ_f. It is also necessary to relate Z_s to T_f for that purpose, and, with this result, it can be shown from (16) and (17) that

$$Z_s = 1 - T_L/(2T_f - T_0 - T_\infty). \tag{29}$$

Equation (26), along with the boundary conditions that $\mathrm{d}\varphi/\mathrm{d}\zeta$ approaches 1 as ζ approaches ∞ and -1 as ζ approaches $-\infty$, defines the well-known problem for the partial-burning regime, the solution to which [24] results in $\Delta = 2$. Equations (27) and (28) therefore imply that

$$Y_{Kf} = [W_K\chi_f(2T_f - T_0 - T_\infty)^2 T_a]/[W_\infty T_f^2 T_Q A \mathrm{e}^{-T_a/T_f}]. \tag{30}$$

These result provide all of the information that is needed from the solution to the inner problem.

8. Outer mass fractions at the flame

Integration of (12)–(14) across the flame sheet provides, with use of (15), relationships between the jump conditions for the gradients at the flame sheet. If square brackets identify the difference between the derivative at the flame for $Z > Z_f$ and that for $Z < Z_f$, then, from (17) and (28)

$$\left[\frac{\mathrm{d}T}{\mathrm{d}Z}\right] = -2(2T_f - T_0 - T_\infty). \tag{31}$$

Use of this result along with (15) in integrals of (13) and (14) across the flame sheet yields

$$\begin{aligned}
&\left[\frac{\mathrm{d}Y_O}{\mathrm{d}Z}\right] = \frac{2W_O(2T_f - T_0 - T_\infty)}{W_\infty T_Q}, \qquad \left[\frac{\mathrm{d}Y_F}{\mathrm{d}Z}\right] = \frac{2W_F L(2T_f - T_0 - T_\infty)}{W_\infty T_Q},\\
&\left[\frac{\mathrm{d}Y_I}{\mathrm{d}Z}\right] = \left(\frac{W_K Y_{If}(Q\mathrm{e}^{-T_q/T_f} + H\mathrm{e}^{-T_h/T_f})}{W_I Y_{Kf} A\mathrm{e}^{-T_a/T_f}} - 1\right)\frac{2W_I L(2T_f - T_0 - T_\infty)}{W_\infty T_Q},\\
&\left[\frac{\mathrm{d}Y_K}{\mathrm{d}Z}\right] = \frac{2W_K L(2T_f - T_0 - T_\infty)}{W_\infty T_Q}.
\end{aligned} \tag{32}$$

In the formula for species I, the rate parameters for step 5, 2.0×10^{12} s^{-1} and 12,090 K, are denoted by Q and T_q, respectively, the ratio ω_5/ω_4 at the flame having been introduced directly, avoiding addressing the inner problem for that species. The influence of step 6 has been taken into account in a similar manner; in employing the R steady state to express its concentration in terms of the I concentration, the effective activation temperature T_h, being 15,110 K - 8360 K = 6750 K, arises, with an effective prefactor equal to the product of the prefactors of steps 6 and 3 divided by the rate constant of step 2, giving $H = 5.6\times10^8$ s^{-1}. When these results are employed in the derivatives of (18)–(20) and (23), all values Y_{if} become related to T_f after use is made of $\mathrm{d}\tilde{Z}/\mathrm{d}Z = L(1-Z)^{L-1}$ in (23).

From the first equation in (32) and the derivartive of (18), it may be shown that

$$Y_{Of} = \frac{T_f - T_0}{T_f - (T_0 + T_\infty)/2}\left[\frac{Y_{O\infty}}{2} - \frac{W_O(T_f - T_\infty)}{W_\infty T_Q}\right]. \tag{33}$$

The derivative of (19) can be treated in a similar manner to obtain an expression for Y_{Ff} from the second equality in (32), but that result will not be written here since Y_{Ff} does not appear anywhere in the analysis. An expression for Y_{If}, however, is needed, and from the third expression in (32) it is found by taking the derivative of (20) that Y_{If} is related to Y_{Kf} according to

$$Y_{If} = \frac{2\tilde{Z}_f W_I(T_f - T_0)}{W_\infty T_Q}\left[1 + \frac{2\tilde{Z}_f W_K(T_f - T_0)(Q\mathrm{e}^{-T_q/T_f} + H\mathrm{e}^{-T_h/T_f})}{W_\infty T_Q Y_{Kf} A\mathrm{e}^{-T_a/T_f}}\right]^{-1}. \tag{34}$$

Finally, with the shorthand notation $R = 1 - \tilde{Z}_f$ and $S = 1 - \tilde{Z}_s$, it can be shown from the derivative of (23) that

$$Y_{Kf} = C(1-R)(R - S^2) - 2W_K(T_f - T_0)(1-R)/(W_\infty T_Q). \tag{35}$$

9. The variation of the flame temperature with the most relevant inverse residence time at the flame

The most relevant inverse residence time at the flame for describing the the droplet history is χ_f because the heat transfer controls the droplet behaviour, so it is desirable to use the formula given above equation (21) to relate $\tilde{\chi}_f$ in (22) to χ_f. Substitution of (30) into (34) and of (22) and (30) into (35) then results in (34) and (35) becoming two independent equations involving the three unknowns Y_{If}, χ_f, and T_f, when (33) is employed for Y_{Of} and (28) and (29) are used, the tilde variables being related to Z as previously indicated. Elimination of the first of the three variables from the two equations then leads to a quadratic equation for χ_f as a function of T_f, the positive solution to which is

$$\chi_f = \frac{(1-R)(T_f - T_0)T_f^2(A\mathrm{e}^{-T_a/T_f} + Q\mathrm{e}^{-T_q/T_f} + H\mathrm{e}^{-T_h/T_f})}{T_a(2T_f - T_0 - T_\infty)^2}[(1+E)^{1/2} - 1], \tag{36}$$

in which

$$E = \frac{(R-S^2)T_a(T_f - T_0)(Y_{Of}\rho_f/W_O)B\mathrm{e}^{T_b/T_f}}{T_f^2(A\mathrm{e}^{-T_a/T_f} + Q\mathrm{e}^{-T_q/T_f} + H\mathrm{e}^{-T_h/T_f})^2/(A\mathrm{e}^{-T_a/T_f})} - \frac{4A\mathrm{e}^{-T_a/T_f}(Q\mathrm{e}^{-T_q/T_f} + H\mathrm{e}^{-T_h/T_f})}{(A\mathrm{e}^{-T_a/T_f} + Q\mathrm{e}^{-T_q/T_f} + H\mathrm{e}^{-T_h/T_f})^2}. \tag{37}$$

It is noteworthy that the value of T_Q affects these results only through the factor Y_{Of} in E, that is, the heat release influences the value of the inverse residence time at any given flame temperature only by modifying the oxygen concentration in the inner flame zone during combustion in a given atmosphere, so that, in the approximation suggested after Equation (33), the heat release (which, of course, is essential to the cool flame) does not affect predictions of the droplet behaviour, helping to support the utility of the chemistry in Table 1 even when the energetics are not described well.

There is a temperature above which E becomes negative and the present chemical-kinetic description no longer applies; the value of E increases with decreasing flame temperature below this limiting value but soon reaches a maximum and decreases continually thereafter. The maximum value of E is small enough that an expansion of the square root about $E=0$ is accurate over the entire temperature range of interest, resulting in the simplified equation

$$\chi_f = \frac{(1-R)(R-S^2)(T_f - T_0)^2(Y_{Of}\rho_f/W_O)B\mathrm{e}^{T_b/T_f}A\mathrm{e}^{-T_a/T_f}}{2(2T_f - T_0 - T_\infty)^2(A\mathrm{e}^{-T_a/T_f} + Q\mathrm{e}^{-T_q/T_f} + H\mathrm{e}^{-T_h/T_f})} - \frac{2(1-R)(T_f - T_0)T_f^2A\mathrm{e}^{-T_a/T_f}(Q\mathrm{e}^{-T_q/T_f} + H\mathrm{e}^{-T_h/T_f})}{T_a(2T_f - T_0 - T_\infty)^2(A\mathrm{e}^{-T_a/T_f} + Q\mathrm{e}^{-T_q/T_f} + H\mathrm{e}^{-T_h/T_f})}, \tag{38}$$

expressing the importance of step 3 in increasing the heat-release rate at the lower temperatures (lessening the influence of step 4) and of steps 5 and 6 in decreasing it at higher temperatures.

The plot in Figure 2 shows χ_f as a function of T_f for heptane droplets in air at normal atmospheric conditions for two different values of L, obtained from (36) and (37) by using (33) with $T_Q = 4{,}000$ K (employing the heptane values $\rho_\infty = 1.164$ kg/m^3, $T_s = 372$ K, and $T_L = 120$ K). The value of T_Q selected here might seem large, but that is merely

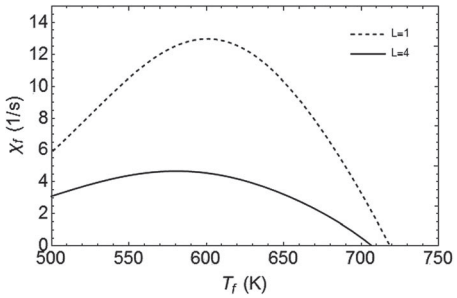

Figure 2. Predicted dependence of the inverse residence time on the flame temperature for n-heptane droplets in an atmosphere of air at 1 atm and 300 K, with $L = 4$ and with $L = 1$.

an artifact of the normalisation; computational studies [20] have shown that the principal cool-flame products are CO and H_2O, along with lesser amounts of CH_2O, C_2H_4, and H_2O_2, and with the heat release taken to be that produced in combustion to CO and H_2O, for heptane this is the value rounded to one significant figure, rounded downward because the other products involve less heat release. Values of temperatures below the maximum of these curves (the left part of the figure) represent conditions in the low-temperature, unstable range, the maximum corresponding to cool-flame extinction conditions. Comparison of the curve for $L = 4$ with that for $L = 1$ demonstrates the substantial reduction in the level of the inverse time scale (implying a longer residence time) for an improved (larger) value of the Lewis number of K is employed. The difference is around a factor of four, roughly proportional to the Lewis-number ratio.

10. Lewis-number effects

Lewis numbers influence the predictions of the present analysis and of the previous asymptotic analysis differently. Although the previous publication [22] is restricted to Lewis numbers of unity, it is straightforward to calculate the Lewis-number influence on those predictions. In that theory, the chemistry occurring in the vicinity of the crossover temperature involves only the species K, so that the Lewis number of that species would appear on the right-hand side of the first equation of the paper. That factor is then carried through the rest of the analysis without any other modification and results in the predicted value of the inverse residence time at extinction being proportional to the Lewis number, the opposite of the dependence in (38), where the dominant Lewis-number-dependent factor $R = [(T_f - T_0)/(T_f - T_0 - T_\infty)]^L$ (the S^2 term being negligible) decreases with increasing Lewis numbers, The value of the inverse residence time at the flame for $L = 4$ in the earlier analysis thus would exceed that for $L = 1$, contrary to what is seen in Figure 2.

The reason for the difference resides in the different flame structures for the two different theories. In the earlier work, all of the chemistry occurred in a narrow reaction zone, and increasing the Lewis number decreased the loss rate of the important reactant K produced there, thereby making the chemistry more robust and resistant to extinction, so that extinction is delayed until a shorter residence time in the reaction zone is achieved, corresponding to a larger value of χ_f. By way of contrast, in the present chemistry the important species K is produced in a large distributed-reaction region, and it must diffuse into the narrow heat-release zone to support the reaction there. Increasing the Lewis number of

K reduces the rate at which it can diffuse into the hottest zone, thereby decreasing the heat-release rate and causing extinction to occur earlier in time during droplet combustion, when the droplet is larger so that the value of χ_f is smaller.

11. The extinction diameter

Since the quasi-steady mass-loss rate of the droplet has been denoted by $4\pi\mu$, according to a mass balance the burning-rate constant K (the time rate of decrease of the square of the droplet diameter) is $K = 16\,\mu/(\rho_l d_l)$, where ρ_l is the density of the liquid droplet and d_l is its diameter. It then follows directly from (9) and (10) that

$$\chi = \frac{(K^2/D_\infty)(\rho_l/\rho_\infty)^2(T/T_\infty)(1-Z)^2}{8d_l^2(r/r_s)^4[(\rho D)/(\rho_\infty D_\infty)]}, \tag{39}$$

which, besides depending on the liquid density and properties in the ambient atmosphere, also exhibits explicit dependencies on the burning-rate constant, the droplet diameter, the mixture fraction, the temperature ratio, the radius ratio (r/r_s), and the (ρD) ratio, although this last ratio is unity in the present analysis. The radius ratio here becomes the flame-standoff ratio (r_f/r_s) when evaluated at $\chi = \chi_f$, whence the maximum value of χ_f, that is, χ_{fe} (the subscript e identifying the values of all variables at this maximum), provides an expression for the minimum diameter, which is the extinction diameter, that involves the burning-rate constant, the liquid and ambient properties, and the flame-standoff ratio.

$$d_{le}^2 = \frac{(\rho_l/\rho_\infty)^2(K^2/D_\infty)(T_{fe}/T_\infty)(T_{fe}-T_0)^2}{8(r_{fe}/r_s)^4(2T_{fe}-T_0+T_\infty)^2\chi_{fe}}, \tag{40}$$

where use has been made of (28). One approach to data analysis would be to employ the measured burning-rate constant K and flame-standoff ratio (r_f/r_s) at the time of cool-flame extinction, along with the calculated value of χ_{fe} (the value at the maximum of the curve in the second figure) in this formula to determine a theoretical extinction diameter for comparison with the experimentally measured extinction diameter. The theory, however, also provides expressions for these other two measurable parameters.

12. The burning-rate constant and the flame-standoff ratio

With (ρD)constant, the expressions for the burning-rate constant and for the flame-standoff ratio are $K = [8(\rho_\infty D_\infty)/\rho_l]\ln[1/(1-Z_s)]$ and $(r_f/r_s) = [\ln(1-Z_s)]/[\ln(1-Z_f)]$, obtainable from the analysis in Section 5. Use of (28) and (29) in these expressions provides the results

$$K = [8(\rho_\infty D_\infty))/\rho_l]\ln[(2T_f - T_0 - T_\infty)/T_L] \tag{41}$$

and

$$r_f/r_s = \ln[(2T_f - T_0 - T_\infty)/T_L]/\ln[(2T_f - T_0 - T_\infty)/(T_f - T_0)]. \tag{42}$$

Predicted values of the burning-rate constant (using $\rho_l = 614$ kg/m^3, $\rho_\infty = 1.164$ kg/m^3, and $D_\infty = 2.76\times10^{-5}$ m^2/s) and of the flame-standoff ratio for heptane are shown in Figure 3 for the conditions of Figure 2. These values are seen to vary little over the

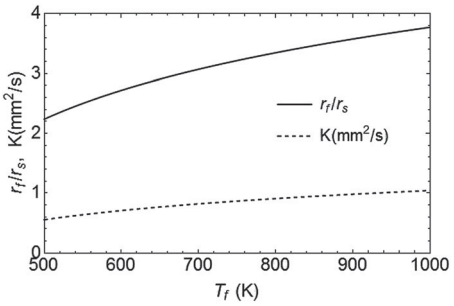

Figure 3. Predicted dependence of the burning-rate constant and of the flame-standoff ratio on the flame temperature for heptane droplets burning in air at normal atmospheric conditions.

flame-temperature range encountered during cool-flame burning, and, moreover, they are comparable with the values found experimentally, the experimental flame-standoff ratio, somewhat dependent on the manner in which it is defined during data reduction, being around 3, and the burning-rate constant around 0.5 mm^2/s, a little less than is seen in the figure.

13. Comparisons with experimental droplet diameters at extinction

Experimental values of droplet diameters at cool-flame extinction are now available for a number of normal alkanes in different atmospheres. Comparisons of predictions with measurements for heptane in oxygen-nitrogen atmospheres at 1 atm and 300 K for various degrees of dilution [15] are shown in Figure 4. The computations employ Equation (40), selecting the maximum of the χ_f curve calculated from Equation (38) with $T_Q = 4{,}000$ K in (33), for the reason explained previously. The prediction for the selection $L = 4$ is seen to fall about in the centre the scatter of the data or slightly above, while that for $L = 1$ seems somewhat low. This observation lends support to the importance of employing correct Lewis numbers in the analysis, with the general agreement suggesting that the approximations that have been introduced, as well as the thermodynamic and reaction-rate parameters that have been employed for n-heptane, are reasonably accurate. Despite the evident scatter of this data, which likely is not entirely random but instead may reflect systematic dependencies on initial droplet diameters and ignition

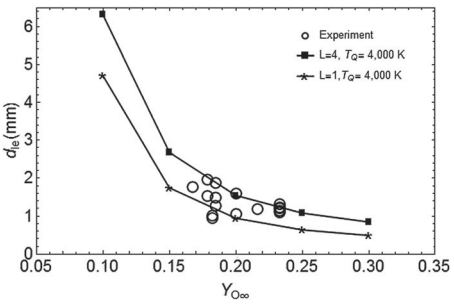

Figure 4. Dependence of the droplet diameter at cool-flame extinction on the oxygen mass fraction in the ambient atmosphere for heptane.

conditions that are yet to be clarified, the experimental results clearly support the predicted increase of the extinction diameter with decreasing oxygen concentration of the atmosphere.

Data like that in Figure 4 for extinction diameters are available for decane droplets at both 1 atm and 1/2 atm [15]. That data, however, are too few and scattered to reveal a systematic dependence on the oxygen mass fraction. The computed values for decane, employing the same rate parameters as those in Table 1 for heptane (since corresponding rate parameters are not available for decane), with other parameters revised to apply to decane, such as, roughly, $T_L = 100$ K (and sill $T_Q = 4{,}000$ K, as the best estimate for decane), lead to results lying somewhat above the centre of the range of the experimental data at both pressures, as might be expected if the true rate parameters for decane were larger than those for heptane. This outcome is favourable for the validity of the theory in that differences in rate parameters for these two fuels are not likely to be large, less than the uncertainties in individual values, the rate of the decomposition step 4, for example, being about the same, while rates of oxygen addition, such as step 3, being somewhat greater because of the larger number of addition sites. These agreements, however, are not definitive because of insufficient data.

When the same rate data are used for different alkanes, the theory predicts a noticeable increase in the extinction diameter with increasing size of the fuel molecule, which is not borne out experimentally, likely because of an increase in the overall rate of the low-temperature chemistry with an increasing number of carbon atoms in the normal alkane, along with initiation of intrusion of fuel-pyrolysis processes that lead to (observed) sooting increases with increasing fuel molecular weight and pressure. These explanations unfortunately cannot be tested here because the extensive degree of reduction of the chemistry in Table 1 is not yet available for alkanes higher than heptane, and accounting for the second would require much more chemistry. The appreciable scatter of the data, as may be seen in Figure 4, for example, may be associated with the shapes of the curves in Figure 2, with small perturbations leading to extinctions not occurring precisely at the maximum point, whence it could be helpful if much more extensive sets of experimental data could be obtained.

More recent experimental results are available for the dependence of extinction diameters on pressure at a fixed ambient oxygen mass fraction for droplets of dodecane, which, with nearly twice as many oxygen addition sites on the alkyl radical as heptane, may be expected to have noticeably faster low-temperature chemistry (although differences may not be large enough to preclude use of the parameters in Table 1 for purposes of comparison, which is done here in the absence of corresponding rate data for dodecane). The experiments, performed in a 300 K atmosphere of oxygen and nitrogen having an oxygen mass fraction of 0.23, exhibited droplet diameters at extinction which are shown along with the theoretical results in Figure 5. Calculated by employing the estimated T_Q value for dodecane, again 4,000 K, along with the pressure-dependent boiling temperature (about 490 K at 1 atm) and the measure T_L of the heat of vaporisation (90 K at 1 atm and decreasing with increasing pressure), these predicted extinction diameters are found to exceed those measured by amounts increasing with pressure, starting from a factor of 4 at the lowest pressure. Although an increase in the value of T_Q would improve the agreement considerably, good justification for such an increase is lacking. The difference observed at the lowest pressure is consistent with the chemistry being faster for dodecane; increasing the value of B by a factor of 5 and A by a factor of 2, for example, would produce agreement. The experimental pressure dependence is, however, stronger than predicted,

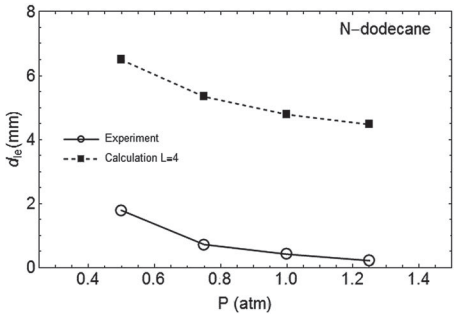

Figure 5. Dependence of the droplet diameter at cool-flame extinction on pressure for dodecane.

indicating that more extensive modifications of the chemistry are likely to be needed for higher alkanes such as dodecane at elevated pressures.

14. Extinction-diameter scaling and the limiting oxygen index

Scaling laws have been addressed for the dependence of the diameter of the fuel droplet at cool-flame extinction on the oxygen concentration in the ambient atmosphere. In the approximation that extinction occurs at the crossover temperature in the NTC range, the values of the activation energies of steps 4 and 6 of Table 1 enter into the scaling and lead to the prediction that the extinction diameter varies approximately as the $-3/4$ power of the oxygen concentration [15]. The previous asymptotic analysis [22] resulted in that dependence being related differently to the variation of the crossover temperature with the oxygen concentration and effectively changed the approximate power law from $-3/4$ to $-1/2$. Both of these dependencies, however, appear to be weaker than what is observed experimentally.

If the last term is neglected in Equation (38) and use is made of the observation that the flame temperature at extinction is calculated to be approximately the same for all of the oxygen concentrations addressed, then the droplet diameter at extinction is found from (33), (38), and (40) to be proportional to $([O_2] - \alpha)^{-1/2}$, where $\alpha = (2\rho_f/W_\infty)(T_f - T_\infty)/T_Q$ is independent of the oxygen concentration $[O_2]$ (but proportional to pressure) if T_Q is constant (likely the most reasonable choice). As α approaches zero, this scaling becomes the same as that of the previous asymptotic analysis, but the dependence becomes stronger as the value of α increases, and, in addition, from (38) it is seen that the last term further strengthens this dependence by increasing the sensitivity to this factor. The present results thus do not yield a simple power-law scaling but predict instead an increasingly strong dependence of the extinction diameter on $[O_2]$ as it decreases, a dependence that becomes more pronounced as the heat release in the flame is reduced.

With all other parameters fixed, there is, in fact, no solution for the flame structure if the ambient oxygen concentration is too small ($[O_2] < \alpha$), according to Equation (33), because more oxygen would then have to be consumed at the hot flame than is available. This implies the existence of a limiting oxygen index (LOI) for cool-flame-supported droplet combustion, below which burning ceases to occur. The rate of change of the droplet extinction diameter with the ambient oxygen concentration becomes infinite as the LOI is approached. The value of the ambient oxygen mass fraction at the LOI is readily obtained

from (33). Because of the likely decrease in the flame temperature with increasing dilution, in an atmosphere of oxygen and nitrogen at 300 K, use of 4,000 K for T_Q, the estimated value for heptane, would give an oxygen mole fraction in the ambient atmosphere on the order of 0.1 at the LOI. This value is below the value at the LOI of the hot flame, suggesting the possibility of cool-flame-supported droplet combustion in atmospheres with insufficient oxygen to support hot flames. Unfortunately the uncertainty in the value of the empirical heat-release measure T_Q leads to uncertainty in the value of the LOI, which may differ for different normal alkanes and may or may not be high enough to be readily measured, but the existence of an LOI is a robust prediction of the analysis.

15. Conclusions

It may be concluded from this study that, when reasonable values of the Lewis numbers of the important reaction intermediates are taken into account, and proper energetics for cool-flame combustion of normal-alkane fuels to carbon monoxide and water vapour are included, then six elementary reaction steps, with two of the species involved (the hydroxyl and initially formed alkyl radicals) obeying accurate chemical-kinetic steady-state approximations, provide good predictions of the quasi-steady cool-flame stage of droplet combustion and its extinction conditions at and below normal atmospheric pressure. That combustion involves a flame structure in which three unimolecular steps with high activation energies, decomposition of alkylketohydroperoxide generating hydroxyl, decomposition of hydroperoxylkyl to the comparatively unreactive hydroperoxyl and conjugate alkene, and carbon-carbon bond breaking of the alkyl radical (as occurs in high-temperature combustion), all proceed in a narrow reaction zone at the highest temperature, while the absolutely essential intermediate, alkylketohydroperoxide, is produced in a distributed manner, throughout practically all of the gas phase, by a step with an activation energy that is effectively negative in the NTC range. This alkylketohydroperoxide then diffuses to the thin, hottest reaction zone, where it is consumed and where all of the heat is liberated. This flame structure is described well by activation-energy asymptotics of the partial-burning regime, different from an earlier analysis of that type, which treated only one reaction occurring in the thin zone, excluding the distributed reaction.

The asymptotic analysis predicts values of droplet burning-rate constants and flame-standoff ratios that agree reasonably well with experiment. It also predicts that the inverse residence time in the flame achieves a maximum value for a flame temperature between 600 K and 800 K, corresponding to cool-flame temperatures in the range found by detailed computational investigations employing chemical mechanisms with hundreds or thousands of elementary steps. The maximum of the inverse residence time corresponds to a minimum droplet diameter for which flame-structure solutions exist. This minimum diameter is expected to be close to the droplet diameter at which cool-flame extinction occurs. Comparisons of predicted values of extinction diameters with values measured in experiments performed aboard the ISS for normal heptane droplets, normal decane droplets, and normal dodecane droplets exhibit general agreement as well as showing the observed decrease of the extinction diameter with increasing oxygen concentration of the atmosphere and with increasing pressure at a fixed oxygen mass fraction. All of the aforementioned elements of the theory must be included to achieve this agreement, and the differences that are observed can be attributed to likely differences in values of reaction-rate parameters that have not yet been well determined and to the onset of sooting effects at higher pressures. The six

pseudo-elementary irreversible reaction steps, with rate parameters justified as much as possible at present by independent chemical-kinetic investigations, as well as accounting for the Lewis numbers of intermediates being greater than unity, therefore are essential in a minimal description for quantitative understanding of cool-flame-supported normal-alkane droplet combustion, and they lead to the requirement that, for the oxygen concentration to be positive in the hot reaction zone, the ambient oxygen concentration must exceed a value determined by the heat release and the flame temperature that establishes a limiting oxygen index.

Acknowledgments

The Flammability-Limit-Experiment (FLEX) project on ISS produced the experimental and computational results with which we compared our predictions, and we are indebted to the FLEX engineering and science teams for their invaluable contributions. We also especially wish to thank D. L. Dietrich, not only for his expert data acquisition and reduction, but also for his helpful ideas and observations throughout this study.

Disclosure statement

No potential conflict of interest was reported by the author(s).

Funding

This research was supported by the NASA Space Life and Physical Sciences Research and Applications Program. Some of the most recent effort of the first author was supported by the National Science Foundation through Grant CBET-1740499.

References

[1] E. Ranzi, P. Gaffuri, T. Faravelli, and P. Dagaut, *A wide-range modelling study of n-heptane oxidation*, Combust. Flame. 103 (1995), pp. 91–106.
[2] H.J. Curran, P. Gaffuri, W.J. Pitz, and C.K. Westbrook, *A comprehensive modeling study of n-heptane oxidation*, Combust. Flame. 114 (1998), pp. 149–177.
[3] C.K. Westbrook, W.J. Pitz, O. Herbinet, H.J. Curran, and E.J. Silke, *A comprehensive detailed chemical kinetic reaction mechanism for combustion of n-alkane hydrocarbons from n-octane to n-hexadecane*, Combust. Flame. 156 (2009), pp. 181–199.
[4] A. Cuoci, M. Mehl, G. Buzzi-Ferraris, T. Faravelli, D. Manca, and E. Ranzi, *Autoignition and burning rates of fuel droplets under microgravity*, Combust. Flame. 143 (2005), pp. 211–226.
[5] V. Nayagam, D.L. Dietrich, P. Ferkul, M.C. Hicks, and F.A. Williams, *Can cool flames support quasi-steady alkane droplet burning?*, Combust. Flame. 159 (2012), pp. 3583–3588.
[6] S. Saxena and I.D. Bedoya, *Fundamental phenomena affecting low temperature combustion and HCCI engines, high load limits and strategies for extending these limits*, Prog. Energy. Combust. Sci. 145 (2013), pp. 457–488.
[7] R.D. Reitz, *Directions in internal combustion research*, Combust. Flame. 160 (2013), pp. 1–8.
[8] T.I. Farouk and F.L. Dryer, *Isolated n-heptane droplet combustion in microgravity: "cool flames" two-stage combustion*, Combust. Flame. 161 (2014), pp. 565–581.
[9] A. Cuoci, A. Frassoldati, T. Faravelli, and E. Ranzi, *Cool Flames in Droplet Combustion*, in *XXXVI Meeting of the Italian Section of the Combustion Institute*, 2013
[10] T.I. Farouk, M.C. Hicks, and F.L. Dryer, *Multistage oscillatory "Cool Flame" behavior for isolated alkane droplet combustion in elevated pressure microgravity condition*, Proc. Combust. Inst. 35 (2015), pp. 1701–1708.
[11] T.I. Farouk, D. Dietrich, F.E. Alam, and F.L. Dryer, *Isolated n-decane droplet combustion - dual stage and single stage transition to "cool flame" droplet burning*, Proc. Combust. Inst. 36 (2017), pp. 2523–2530.

[12] A. Cuoci, A.E. Saufi, A. Frassoldati, D.L. Dietrich, F.A. Williams, and T. Faravelli, *Flame extinction and low-temperature combustion of isolated fuel droplets of n-alkanes*, Proc. Combust. Inst. 36 (2017), pp. 2531–2539.
[13] T.I. Farouk, D. Dietrich, and F.L. Dryer, *Three stage cool flame droplet burning behavior of n-alkane droplets at elevated pressure conditions*, Proc. Combust. Inst.37 (2019), pp. 3353–3361.
[14] D.L. Dietrich, V. Nayagam, M.C. Hicks, P.V. Ferkul, F.L. Dryer, T. Farouk, B.D. Shaw, H.K. Suh, M.Y. Choi, Y.C. Liu, C.T. Avedisian, and F.A. Williams, *Droplet combustion experiments aboard the international space station*, Microgravity. Sci. Technol. 26 (2014), pp. 65–76.
[15] V. Nayagam, D.L. Dietrich, M.C. Hicks, and F.A. Williams, *Cool-flame extinction during n-alkane droplet combustion in microgravity*, Combust. Flame. 162 (2015), pp. 2140–2147.
[16] Y.C. Liu, Y. Xu, M.C. Hicks, and C.T. Avedisian, *Comprehensive study of initial diameter effects and other observations on convection-free droplet combustion in the standard atmosphere for n-heptane, n-octane, and n-decane*, Combust. Flame. 171 (2016), pp. 27–41.
[17] V. Nayagam, D.L. Dietrich, and F.A. Williams, *Partial-burning regime for quasi-steady droplet combustion supported by cool flames*, AIAA J. 54 (2016), pp. 1235–1239.
[18] D.L. Dietrich, R. Calabria, P. Massoli, V. Nayagam, and F.A. Williams, *Experimental observations of the low-temperature burning of decane/hexanol droplets in microgravity*, Combust. Sci. Technol. 189 (2017), pp. 520–554.
[19] N. Peters, G. Paczko, R. Seiser, and K. Seshadri, *Temperature cross-over and non-thermal runway at two-stage ignition of n-heptane*, Combust. Flame. 128 (2002), pp. 38–59.
[20] G. Paczko, N. Peters, K. Seshadri, and F.A. Williams, *The role of cool-flame chemistry in quasi-steady combustion and extinction of n-heptane droplets*, Combust. Theory Model. 18 (2014), pp. 515–531.
[21] J.C. Prince, F.A. Williams, and G.E. Ovando, *A short mechanisms for the low-temperature ignition of n-heptane at high pressures*, Fuel 149 (2015), pp. 138–142.
[22] K. Seshadri, N. Peters, F.A. Williams, V. Nayagam, and G. Paczko, *Asymptotic analysis of quasi-steady n-heptane droplet combustion supported by cool-flame chemistry*, Combust. Theory Model. 20 (2016), pp. 1118–1130.
[23] J.C. Prince and F.A. Williams, *Short chemical-kinetic mechanisms for low-temperature ignition of propane and ethane*, Combust. Flame. 159 (2012), pp. 2336–2344.
[24] A. Liñán, *The asymptotic structure of counterflow diffusion flames for large activation energies*, Acta. Astronaut. 1 (1974), pp. 1007–1039.
[25] P. Gaffuri, T. Faravelli, E. Ranzi, N.P. Cernensky, D. Miller, A. d'Anna, and A. Ciajolo, *Comprehensive kinetic model for the low-temperature oxidation of hydrocarbons*, AIChE J. 43 (1997), pp. 1278–1286.
[26] J.C. Prince and F.A. Williams, *Revised short mechanisms for low-temperature ignition of n-hepane for a wider pressure range*, Fuel 150 (2015), pp. 730–731.
[27] B.D. Shaw and J.B. Wei, *Influence of gravity and ambient pressure on combustion and flammability of n-heptane and 1-propanol droplets in air-diluent environments*, Combust. Sci. Technol. 183 (2011), pp. 969–983.
[28] A.L. Sanchez and F.A. Williams, *Recent advances in understanding of flammability characteristics of hydrogen*, Prog. Energy. Combust. Sci. 41 (2014), pp. 1–55.
[29] C.K. Law and F.A. Williams, *Kinetics and convection in the combustion of alkane droplets*, Combust. Flame. 19 (1972), pp. 393–405.